

Calibration of cryogenic amplification chains using normal-metal–insulator–superconductor junctions

E. Hyppä,¹ M. Jenei,¹ S. Masuda,^{2,1} V. Sevriuk,¹ K. Y. Tan,^{1,3} M. Silveri,^{1,4} J. Goetz,¹ M. Partanen,¹ R. E. Lake,¹ L. Grönberg,⁵ and M. Möttönen¹

¹*QCD Labs, QTF Centre of Excellence, Department of Applied Physics, Aalto University, P.O. Box 13500, FI-00076, Aalto, Finland*

²*College of Liberal Arts and Sciences, Tokyo Medical and Dental University, Ichikawa, 272-0827, Japan*

³*Center for Quantum Computation and Communication Technology, School of Electrical Engineering and Telecommunications, University of New South Wales, Sydney, NSW 2052, Australia*

⁴*Research Unit of Nano and Molecular Systems, University of Oulu, P.O. Box 3000, FI-90014, Oulu, Finland*

⁵*VTT Technical Research Centre of Finland, QFT Center of Excellence, P.O. Box 1000, FI-02044, Aalto, Finland*

Various applications of quantum devices call for an accurate calibration of cryogenic amplification chains. To this end, we present a convenient calibration scheme and use it to accurately measure the total gain and noise temperature of an amplification chain by employing normal-metal–insulator–superconductor (NIS) junctions. Our method is based on the radiation emitted by inelastic electron tunneling across voltage-biased NIS junctions. We derive an analytical equation that relates the generated power to the applied bias voltage which is the only control parameter of the device. After the setup has been characterized using a standard voltage reflection measurement, the total gain and the noise temperature are extracted by fitting the analytical equation to the microwave power measured at the output of the amplification chain. The 1σ uncertainty of the total gain of 51.84 dB appears to be of the order of 0.1 dB.

Superconducting circuits provide a promising approach to implement a variety of quantum devices and to explore fundamental physical phenomena, such as the light-matter interaction¹ in the ultrastrong coupling regime². In addition, superconducting circuits are potential candidates for building a large-scale quantum computer^{3,4}: superconducting qubits can be coupled in a scalable way^{5–12}, and both the gate and the measurement fidelity of qubits exceed the threshold required for quantum error correction^{10,13–15}.

Since superconducting quantum circuits typically operate in the single-photon regime, signals are amplified substantially for readout^{3,16–21} using a chain of amplifiers, which is distributed over several temperature stages^{16,17}. In the first stage, a near-quantum-limited amplifier²², such as a Josephson parametric amplifier^{23–26}, is often used to lower the noise temperature of the amplification chain²⁷. As a result of cascading several amplifiers, the uncertainty in the total gain of the amplification chain becomes significant and may complicate, for example, the estimation of the photon number in the superconducting circuit. Therefore, accurate, fast, and simple methods for measuring the total gain of an amplification chain are desirable in the investigation of quantum electric devices.

The gain and the noise temperature of cryogenic amplifiers can be measured, for example, using superconducting qubits^{22,28}, Planck spectroscopy of a sub-kelvin thermal noise source²⁹, and the Y -factor method^{30,31} which utilizes the Johnson–Nyquist noise emitted at different temperatures. In addition to these methods, shot noise^{32,33} sources, such as normal-metal–insulator–normal-metal junctions, can be used to determine the gain and noise temperature of cryogenic amplifiers^{34,35}. However, this method typically requires a calibration measurement of the setup due to impedance mismatch³⁴.

In this paper, we present an accurate alternative calibration scheme for the total gain and noise temperature of an amplification chain by utilizing photon-assisted electron tunneling in normal-metal–insulator–superconductor (NIS) junctions. To date, NIS junctions have been utilized in various applications, which include, for example, cryogenic microwave sources³⁷, thermometers^{38,39}, and the recently developed quantum-circuit refrigerator that cools quantum electric circuits by harnessing photon-assisted electron tunneling^{36,40,41}. Here, we determine the gain and noise temperature of an amplification chain by measuring the power emitted by electrons that tunnel inelastically across NIS junctions. The photon emission of the tunneling electrons can be activated by applying a bias voltage across the NIS junctions. For our analysis, we derive an analytic equation for the generated power in the high-bias regime. The analytic model matches our experimental results, which allows us to determine the gain of the amplification with an uncertainty of the order of 0.1 dB.

We demonstrate the proposed calibration scheme on a sample illustrated in Fig. 1. The device incorporates an SINIS junction which consists of two NIS junctions sharing a common normal-metal electrode. The normal-metal electrode of the tunnel junction is capacitively coupled to a half-wavelength superconducting coplanar-waveguide resonator. The resonator is further capacitively coupled to a transmission line from its other end, which conducts the signal to a three-stage amplification chain. The sample is placed in a dry dilution refrigerator at 10-mK base temperature. Reference 37 details the device fabrication.

The bias voltage V_b across the SINIS junction activates the photon-assisted electron tunneling events which control the mean photon number N_r in the fundamental mode of the resonator. The photon number in turn determines the microwave power emitted to the transmis-

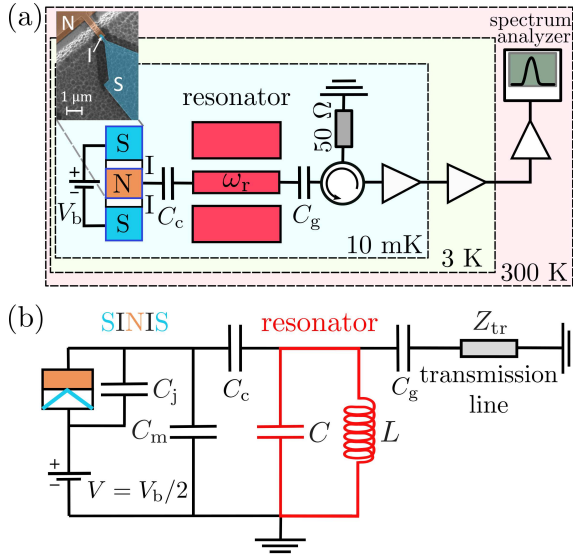


FIG. 1. (a) Schematic measurement setup. A bias voltage V_b is applied across an SINIS junction, which is capacitively coupled (C_c) to a resonator. The bias voltage V_b tunes the photon emission rate of the junction and hence the mean photon number in the weakly coupled resonator³⁶. The other end of the resonator is capacitively coupled (C_g) to a transmission line, which guides the output power to a spectrum analyzer. The inset shows a false-color scanning electron micrograph of a single NIS junction. (b) A simplified electric circuit diagram of the system depicted in (a). The capacitor C_j describes the capacitance of a single NIS junction, whereas the capacitor C_m corresponds to the remaining capacitance. The fundamental mode of the resonator is modeled as an LC oscillator. The characteristic impedance of the transmission line is $Z_{tr} = 50 \Omega$.

sion line. As described in Fig. 2, the electrons can tunnel through the NIS junction either elastically, i.e., without energy exchange with their electromagnetic environment, or inelastically by emitting or absorbing photons. In our setup, the resonator acts as the electromagnetic environment, and consequently the tunneling electrons absorb or emit photons at the resonance frequency of the resonator $f_r = \omega_r/(2\pi) = 4.67$ GHz. For vanishing bias voltage, both the elastic and inelastic tunneling events are suppressed due to the energy gap^{42–44} of 2Δ in the superconductor density of states as shown in Fig. 2(a). If the bias voltage is slightly below the energy gap, i.e., $|eV_b| \lesssim 2\Delta$, electrons can tunnel through the junction by absorbing photons from the environment, which results in cooling of the resonator mode. In this work, we are mostly interested in the high-bias-voltage regime $|eV_b| \gg 2\Delta$, where electron tunneling events involving photon emission are greatly enhanced, and hence the resonator mode heats up. The elevated temperature of the resonator mode leads to an increased radiative power into the transmission line, which enables us to calibrate the total gain of the amplification chain. We show below that the power and the bias voltage relate to each other through a simple equation in

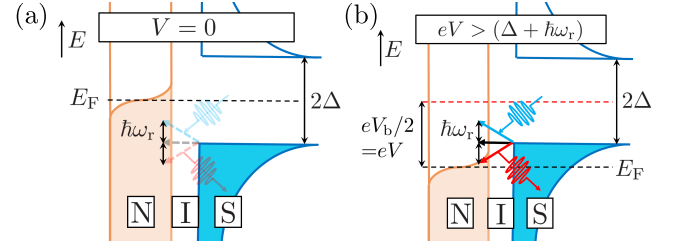


FIG. 2. (a) Sketch of the occupied (shaded) and unoccupied (white) quasiparticle states in an NIS junction at vanishing bias voltage. In the normal metal (orange), the occupation is given by the Fermi–Dirac distribution since the density of states is essentially constant in the energy scale of interest. In the superconducting electrode (blue), there is an energy gap of 2Δ in the density of states, which restricts the possible electron tunneling events. Straight blue arrows indicate tunneling events involving photon (wavy arrow) absorption, whereas red arrows correspond to photon emission, and black arrows depict elastic tunneling events. The low transparency of the arrows highlights that all the above-mentioned tunneling events are suppressed. (b) As (a) but for a bias voltage $eV > \Delta + \hbar\omega_r$ causing the Fermi level E_F of the normal metal (black dashed line) to shift with respect to that of the superconductor (red dashed line). For simplicity, we only show tunneling events originating from the lower edge of the superconductor gap.

the high-bias regime. We apply the theory developed in Ref. 40 to describe the coupling between the resonator and the SINIS junction. In this model, we only take into account single-photon processes and we assume that the quasiparticle temperatures are equal in the normal-metal and superconducting electrodes. Furthermore, we assume sequential tunneling, i.e., that high-order processes are suppressed by the opaque tunnel barrier. Using the simplified electric circuit in Fig. 2(b) and Fermi’s golden rule, we can express the resonator damping rate γ_T and the effective temperature T_T owing to the electron tunneling across the SINIS junction as⁴⁰

$$\gamma_T = \bar{\gamma}_T \frac{\pi}{\omega_r} \sum_{l, \tau = \pm 1} l \vec{F}(\tau eV + l \hbar \omega_r), \quad (1)$$

$$T_T = \frac{\hbar \omega_r}{k_B} \left\{ \ln \left[\frac{\sum_{\tau = \pm 1} \vec{F}(\tau eV + \hbar \omega_r)}{\sum_{\tau = \pm 1} \vec{F}(\tau eV - \hbar \omega_r)} \right] \right\}^{-1}, \quad (2)$$

where $\bar{\gamma}_T$ is the asymptotic damping rate, $\vec{F}(E)$ is the normalized rate of forward tunneling, k_B is the Boltzmann constant, \hbar is the reduced Planck constant, and $V = V_b/2$ is the voltage across a single NIS junction. We also have $\bar{\gamma}_T = 2C_c^2 Z_r \omega_r / [(C_c + C_j + C_m)^2 R_T]$, where $Z_r = \sqrt{L/C}$, R_T is the tunneling resistance of a single NIS junction, and the remaining symbols are defined in Fig. 1(b). The normalized rate of forward tunneling is defined as

$$\vec{F}(E) = \frac{1}{2\pi\hbar} \int d\varepsilon n_S(\varepsilon) \frac{f(\varepsilon - E) - f(\varepsilon)}{1 - e^{-E/(k_B T_N)}}, \quad (3)$$

where E is the energy gained by the tunneling electron, T_N is the temperature of the normal-metal electrode, $f(\varepsilon) = \{\exp[\varepsilon/(k_B T_N)] + 1\}^{-1}$ is the Fermi function, and $n_S(\varepsilon)$ is the Dynes density of states⁴³, which can be written as $n_S(\varepsilon) = |\text{Re}[(\varepsilon + i\gamma_D \Delta)/\sqrt{(\varepsilon + i\gamma_D \Delta)^2 - \Delta^2}]|$. The Dynes parameter γ_D describes the broadening of the superconductor energy gap, and is of the order of $\sim 10^{-4}$ in a typical experimental scenario^{36,37,45}.

In the high-bias regime, $eV \gg \Delta$, we employ Eqs. (1) and (2) to derive the following approximations for the damping rate γ_T and the effective photon number $N_T = \{\exp[\hbar\omega_r/(k_B T_T)] - 1\}^{-1}$ of the engineered environment

$$\gamma_T \approx \bar{\gamma}_T \left[1 + \frac{1}{2} \frac{\Delta^2}{(eV)^2} \right], \quad (4)$$

$$N_T \approx \frac{eV}{2\hbar\omega_r} - \frac{1}{2} - \frac{\Delta^2}{2\hbar\omega_r} \frac{1}{eV}, \quad (5)$$

where we have utilized the Sommerfeld expansion⁴⁶. In addition, we have assumed that the Dynes parameter is small enough to be neglected at high bias voltages.

The resonator exchanges energy with the SINIS junction and with the transmission line. Furthermore, the resonator may be subjected to additional sources of dissipation which we model as a single excess reservoir. Each of these three types of dissipation can be modeled as a virtual transmission line⁴⁷, which allows us to write the net power flow between the resonator and the i th dissipative reservoir as

$$P_i = \hbar\omega_r \gamma_i (N_i - N_r), \quad (6)$$

where γ_i is the damping rate of the resonator owing to the i th reservoir, N_i is the corresponding effective photon number, and N_r is the resulting steady-state occupation of the resonator. Invoking the power balance and using Eqs. (4) and (5), the net power flow into the transmission line can be approximated as

$$P_{\text{tr}} \approx \frac{\gamma_{\text{tr}} \bar{\gamma}_T}{\gamma_{\text{tr}} + \bar{\gamma}_T + \gamma_x} \left\{ \frac{eV}{2} + \hbar\omega_r \left[\frac{\gamma_x (N_x - N_{\text{tr}})}{\bar{\gamma}_T} - N_{\text{tr}} - \frac{1}{2} \right] - \frac{1}{4} \frac{\Delta^2}{eV} \left(1 + \frac{\bar{\gamma}_T}{\bar{\gamma}_T + \gamma_{\text{tr}} + \gamma_x} \right) \right\}, \quad (7)$$

where γ_{tr} and N_{tr} are the damping rate and the effective photon number owing to the transmission line, respectively, whereas γ_x and N_x are the corresponding quantities for the excess losses.

In our experiments, we measure the output power of the amplification chain $P_{\text{out}} = GP_{\text{tr}} + P_{\text{noise}}$, where G is the total gain of the amplification chain including possible attenuation and losses, and P_{noise} is the noise power originating from the amplifiers. Consequently, we can determine the total gain G by fitting a function of the form

$$P_{\text{out}}(V) = aV + b + c/V, \quad (8)$$

to the measured power in the high bias regime $eV \gg \Delta$, where $\{a, b, c\}$ are the fitting parameters. Using Eq. (7),

the total gain G can be expressed in terms of the leading-term coefficient as

$$G = \frac{2a \bar{\gamma}_T + \gamma_{\text{tr}} + \gamma_x}{e \bar{\gamma}_T \gamma_{\text{tr}}}. \quad (9)$$

Although we extract the total gain only from the coefficient a , the other terms in Eq. (8) improve the fit substantially. The effective noise temperature of the amplification chain T_{amp} is obtained by examining the output power at zero bias voltage $P_{\text{out}}(0)$, where P_{tr} is practically zero with our device parameters and consequently

$$T_{\text{amp}} \approx \frac{P_{\text{out}}(0)}{G k_B \Delta f}, \quad (10)$$

where Δf is the bandwidth of the amplification chain.

In our experiments, we characterize the damping rates $\bar{\gamma}_T$, γ_{tr} , and γ_x with high accuracy leaving the parameter a in Eq. (9) as the only free parameter in our model. To this end, we conduct standard microwave reflection measurements at different bias voltages V_b . Based on the input-output theory⁴⁸, the voltage reflection coefficient of our system can be written as⁴⁹

$$\Gamma = \frac{(2-r)\gamma_{\text{tr}} - r(\gamma_T + \gamma_x) + 2ir(\omega_p - \omega_r)}{\gamma_T + \gamma_{\text{tr}} + \gamma_x - 2i(\omega_p - \omega_r)}, \quad (11)$$

where $\omega_p/(2\pi)$ is the probe frequency and r is a complex-valued Fano resonance correction factor, which arises from the direct cross-talk of the dissipative reservoirs⁵⁰.

Since the bias voltage V_b controls the coupling between the electromagnetic environment and the resonator, a Lamb shift arises for the resonance frequency⁴¹ $\omega_r/(2\pi) = 4.67$ GHz. The Lamb shift provides a convenient way of eliminating the unwanted background from the measurement data, namely, normalizing by the zero-bias measurement trace $\Gamma^N(V_b) = \Gamma(V_b)/\Gamma(0)$ as shown in Fig. 3.(a). The ratio of two instances of Eq. (11) is fitted for every V_b above the critical coupling point, $eV_b/(2\Delta) > 1$, where the bias voltage-independent γ_{tr} , γ_x , and the bias voltage-dependent γ_T are fitting parameters. Next, the asymptotic damping rate is extracted using Eq. (4). As a result, our characteristic damping rates are $\gamma_{\text{tr}}/(2\pi) = (1.78 \pm 0.02)$ MHz, $\bar{\gamma}_T/(2\pi) = (17.39 \pm 0.04)$ MHz, and $\gamma_x/(2\pi) = (0.46 \pm 0.01)$ MHz, where the presented 1σ uncertainties are obtained by the following method: First, an error circle is created that has a radius equal to the root mean square fit error and the center is located at $\Gamma^N(V_b, \omega_r)$, which correspond to the resonance of the bias voltage-dependent feature. Finally, confidence intervals of each parameter are individually determined by finding the boundaries such that the fitted Γ^N is located within the error circle. The uncertainty of the excess damping rate is taken as the standard deviation of γ_x over the fitted voltage range.

After measuring the damping rates, we determine the total gain of the amplification chain by recording the microwave power at the output of the amplification chain for different bias voltages across the junction. To this end,

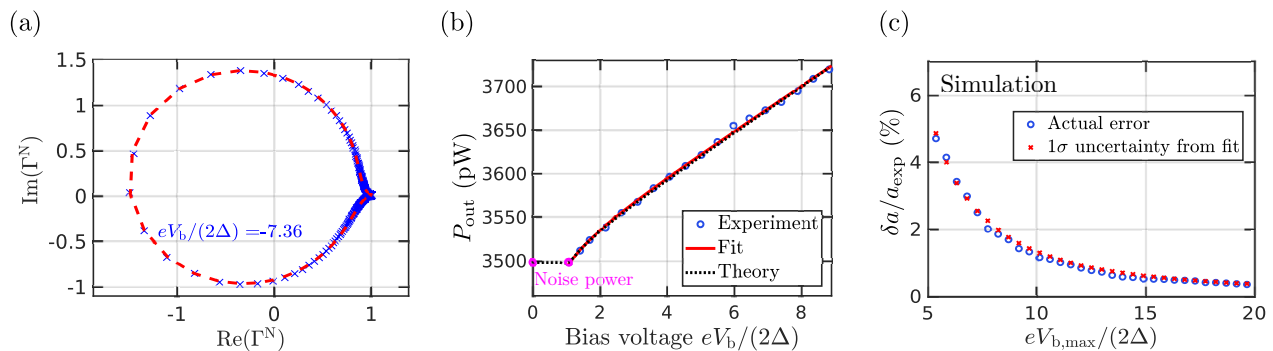


FIG. 3. (a) The normalized complex voltage reflection coefficient Γ^N (blue crosses) and the fit (red dashed line) that is obtained by a nonlinear regression where the ratio of two reflection coefficients of Eq. (11) is fitted. (b) The measured output power P_{out} as a function of the bias voltage (blue dots). The total gain G is fitted using Eq. (8) (red line) in the voltage range $eV_b/(2\Delta) \in [1.07, 8.83]$. The theoretical prediction for the power (dotted black line) is calculated by combining the fitted total gain, Eqs. (1), (2), and (6). The magenta circles illustrate the noise power originating from the amplification chain. Each power data point is averaged over 100 repetitions. (c) The average relative error of the fitting parameter a (blue dots) and the average 1σ uncertainty given by the fit (red crosses) as a function of the upper bound of the fitting range $eV_b/(2\Delta) \in [1.07, eV_{b,\text{max}}/(2\Delta)]$ when Eq. (8) is fitted to 100 simulated power data sets. The simulated power data is obtained by adding normally distributed random noise to the exact theoretical prediction for the power calculated using Eqs. (1), (2), and (6). The standard deviation of the random noise $\sigma = 2.5$ pW and the spacing between consecutive voltage points are chosen to coincide with the data shown in panel (b).

we use a spectrum analyzer and numerically integrate the averaged spectral density around the resonance frequency $\omega_r/(2\pi) = 4.67$ GHz in the range 4.6–4.75 GHz. From the data shown in Fig. 3(b), we observe a monotonous increase of the microwave power if the bias voltage exceeds the energy gap. We finally extract the total gain of the amplification chain by fitting Eq. (8) to the power data. Using Eq. (9) and the experimentally determined device parameters, the total gain of the amplification chain is estimated to be $G = 51.84$ dB. Based on Eq. (10), the average noise temperature of our amplification chain is 11 K in the range 4.6–4.75 GHz.

The relative uncertainty of the fitting parameter a is extracted in the following way: we substitute the damping rates and the calibrated gain into Eq. (9) to determine the expected value a_{exp} for the fitting parameter a . We then create a set of simulated power spectra for bias voltages up to $V_b = 10\Delta/e$. Fitting Eq. (8) to the corresponding power values, we extract the parameter a and record the absolute error $\delta a = a - a_{\text{exp}}$ as a function of the maximum bias $eV_{b,\text{max}}/(2\Delta)$. In addition, we obtain the 1σ uncertainty from the fit and observe that it agrees with the error δa . In our experiments, we reach $eV_b/2\Delta = 9$ and therefore estimate the relative uncertainty of the fitting parameter $\delta a/a_{\text{exp}} = 2\%$. Combining the uncertainties of the damping rates $\bar{\gamma}_T$, γ_{tr} , γ_x , and the fitting parameter a , we acquire 0.10 dB for the uncertainty of the total gain.

In this paper, we have presented a calibration scheme for the total gain and noise temperature of a general amplification chain that comprises cryogenic and non-cryogenic amplifiers. The knowledge of the gain and noise temperature is important when operating quantum devices and other low-power microwave components. Cur-

rently, our setup allows the calibration of the total gain only at frequencies corresponding to a mode frequency of the resonator. The frequency range suitable for calibration can be expanded by placing a superconducting quantum interference device (SQUID) in the resonator^{51,52}. In the future, we aim at benchmarking the accuracy of the proposed gain calibration scheme against a method utilizing a superconducting qubit in a resonator. By employing the ac Stark shift, we can determine the photon number in the resonator^{1,53} and thus the total gain of the amplification chain.

ACKNOWLEDGMENTS

This project has received funding from the European Union’s Horizon 2020 Research and Innovation Programme under the Marie Skłodowska-Curie Grant Agreement No. 795159 and under the European Research Council Consolidator Grant No. 681311 (QUESS), from the Academy of Finland Centre of Excellence in Quantum Technology Grant No. 312300 and No. 305237, from JST ERATO Grant No. JPMJER1601, from JSPS KAKENHI Grant No. 18K03486, and from the Vilho, Yrjö and Kalle Väisälä Foundation. We acknowledge the provision of facilities and technical support by Aalto University at OtaNano - Micronova Nanofabrication Centre.

¹A. Wallraff, D. I. Schuster, A. Blais, L. Frunzio, R.-S. Huang, J. Majer, S. Kumar, S. M. Girvin, and R. J. Schoelkopf, *Nature* **431**, 162 (2004).

²T. Niemczyk, F. Deppe, H. Huebl, E. Menzel, F. Hocke, M. Schwarz, J. Garcia-Ripoll, D. Zueco, T. Hümmer, E. Solano, *et al.*, *Nat. Phys.* **6**, 772 (2010).

³M. H. Devoret and R. J. Schoelkopf, *Science* **339**, 1169 (2013).

- ⁴A. Blais, R.-S. Huang, A. Wallraff, S. M. Girvin, and R. J. Schoelkopf, *Phys. Rev. A* **69**, 062320 (2004).
- ⁵J. Majer, J. Chow, J. Gambetta, J. Koch, B. Johnson, J. Schreier, L. Frunzio, D. Schuster, A. Houck, A. Wallraff, *et al.*, *Nature* **449**, 443 (2007).
- ⁶M. A. Sillanpää, J. I. Park, and R. W. Simmonds, *Nature* **449**, 438 (2007).
- ⁷L. DiCarlo, J. Chow, J. Gambetta, L. S. Bishop, B. Johnson, D. Schuster, J. Majer, A. Blais, L. Frunzio, S. Girvin, *et al.*, *Nature* **460**, 240 (2009).
- ⁸L. DiCarlo, M. D. Reed, L. Sun, B. R. Johnson, J. M. Chow, J. M. Gambetta, L. Frunzio, S. M. Girvin, M. H. Devoret, and R. J. Schoelkopf, *Nature* **467**, 574 (2010).
- ⁹T. Brecht, W. Pfaff, C. Wang, Y. Chu, L. Frunzio, M. H. Devoret, and R. J. Schoelkopf, *npj Quantum Inf.* **2**, 16002 (2016).
- ¹⁰R. Barends, J. Kelly, A. Megrant, A. Veitia, D. Sank, E. Jeffrey, T. C. White, J. Mutus, A. G. Fowler, B. Campbell, *et al.*, *Nature* **508**, 500 (2014).
- ¹¹A. D. Córcoles, E. Magesan, S. J. Srinivasan, A. W. Cross, M. Steffen, J. M. Gambetta, and J. M. Chow, *Nat. Commun.* **6**, 6979 (2015).
- ¹²C. Song, K. Xu, W. Liu, C.-p. Yang, S.-B. Zheng, H. Deng, Q. Xie, K. Huang, Q. Guo, L. Zhang, *et al.*, *Phys. Rev. Lett.* **119**, 180511 (2017).
- ¹³D. S. Wang, A. G. Fowler, and L. C. Hollenberg, *Phys. Rev. A* **83**, 020302 (2011).
- ¹⁴J. Kelly, R. Barends, A. Fowler, A. Megrant, E. Jeffrey, T. White, D. Sank, J. Mutus, B. Campbell, Y. Chen, *et al.*, *Nature* **519**, 66 (2015).
- ¹⁵N. Ofek, A. Petrenko, R. Heeres, P. Reinhold, Z. Leghtas, B. Vlastakis, Y. Liu, L. Frunzio, S. Girvin, L. Jiang, *et al.*, *Nature* **536**, 441 (2016).
- ¹⁶F. Mallet, F. R. Ong, A. Palacios-Laloy, F. Nguyen, P. Bertet, D. Vion, and D. Esteve, *Nat. Phys.* **5**, 791 (2009).
- ¹⁷A. Dewes, F. Ong, V. Schmitt, R. Lauro, N. Boulant, P. Bertet, D. Vion, and D. Esteve, *Phys. Rev. Lett.* **108**, 057002 (2012).
- ¹⁸Z. Lin, K. Inomata, W. Oliver, K. Koshino, Y. Nakamura, J. Tsai, and T. Yamamoto, *Appl. Phys. Lett.* **103**, 132602 (2013).
- ¹⁹D. Riste, M. Dukalski, C. Watson, G. De Lange, M. Tiggelman, Y. M. Blanter, K. W. Lehnert, R. Schouten, and L. DiCarlo, *Nature* **502**, 350 (2013).
- ²⁰J. Heinsoo, C. K. Andersen, A. Remm, S. Krinner, T. Walter, Y. Salathé, S. Gasparinetti, J.-C. Besse, A. Potočnik, A. Wallraff, and C. Eichler, *Phys. Rev. Appl.* **10**, 034040 (2018).
- ²¹J. Ikonen, J. Goetz, J. Ilves, A. Kernen, A. M. Gunyhó, M. Partanen, K. Y. Tan, L. Grönberg, V. Vesterinen, S. Simbierowicz, J. Hassel, and M. Möttönen, *Phys. Rev. Lett.* **122**, 080503 (2019).
- ²²C. Macklin, K. O'Brien, D. Hover, M. Schwartz, V. Bolkhovskiy, X. Zhang, W. Oliver, and I. Siddiqi, *Science* **350**, 307 (2015).
- ²³B. Yurke, P. Kaminsky, R. Miller, E. Whittaker, A. Smith, A. Silver, and R. Simon, *Phys. Rev. Lett.* **60**, 764 (1988).
- ²⁴T. Yamamoto, K. Inomata, M. Watanabe, K. Matsuba, T. Miyazaki, W. Oliver, Y. Nakamura, and J. Tsai, *Appl. Phys. Lett.* **93**, 042510 (2008).
- ²⁵M. Castellanos-Beltran and K. Lehnert, *Appl. Phys. Lett.* **91**, 083509 (2007).
- ²⁶S. Pogorzalek, K. G. Fedorov, L. Zhong, J. Goetz, F. Wulschner, M. Fischer, P. Eder, E. Xie, K. Inomata, T. Yamamoto, Y. Nakamura, A. Marx, F. Deppe, and R. Gross, *Phys. Rev. App.* **8**, 024012 (2017).
- ²⁷R. Kokkonen, J. Govenius, V. Vesterinen, R. Lake, A. Gunyhó, K. Tan, S. Simbierowicz, L. Grönberg, J. Lehtinen, M. Prunnila, *et al.*, arXiv preprint arXiv:1806.09397 (2018).
- ²⁸J. Goetz, S. Pogorzalek, F. Deppe, K. G. Fedorov, P. Eder, M. Fischer, F. Wulschner, E. Xie, A. Marx, and R. Gross, *Phys. Rev. Lett.* **118**, 103602 (2017).
- ²⁹M. Mariani, E. P. Menzel, F. Deppe, M. A. Caballero, A. Baust, T. Niemczyk, E. Hoffmann, E. Solano, A. Marx, and R. Gross, *Phys. Rev. Lett.* **105**, 133601 (2010).
- ³⁰*Noise Figure Measurement Accuracy - The Y-Factor Method*, Agilent Technologies (2001), application note 57-2.
- ³¹J. Fernandez, progress report **42-135** (1998).
- ³²Y. M. Blanter and M. Büttiker, *Phys. Rep.* **336**, 1 (2000).
- ³³L. Spietz, K. Lehnert, I. Siddiqi, and R. Schoelkopf, *Science* **300**, 1929 (2003).
- ³⁴S.-W. Chang, J. Aumentado, W.-T. Wong, and J. C. Bardin, in *Microwave Symposium (IMS), 2016 IEEE MTT-S International* (IEEE, 2016) pp. 1-4.
- ³⁵A. Aassime, G. Johansson, G. Wendin, R. Schoelkopf, and P. Delsing, *Phys. Rev. Lett.* **86**, 3376 (2001).
- ³⁶K. Y. Tan, M. Partanen, R. E. Lake, J. Govenius, S. Masuda, and M. Möttönen, *Nat. Commun.* **8**, 15189 (2017).
- ³⁷S. Masuda, K. Y. Tan, M. Partanen, R. E. Lake, J. Govenius, M. Silveri, H. Grabert, and M. Möttönen, *Sci. Rep.* **8**, 3966 (2018).
- ³⁸S. Kafanov, A. Kemppinen, Y. A. Pashkin, M. Meschke, J. Tsai, and J. P. Pekola, *Phys. Rev. Lett.* **103**, 120801 (2009).
- ³⁹S. Gasparinetti, K. Viisanen, O.-P. Saira, T. Faivre, M. Arzeo, M. Meschke, and J. Pekola, *Phys. Rev. Appl.* **3**, 014007 (2015).
- ⁴⁰M. Silveri, H. Grabert, S. Masuda, K. Y. Tan, and M. Möttönen, *Phys. Rev. B* **96**, 094524 (2017).
- ⁴¹M. Silveri, S. Masuda, V. Sevriuk, K. Y. Tan, M. Jenei, E. Hyppä, F. Hassler, M. Partanen, J. Goetz, R. E. Lake, L. Grönberg, and M. Möttönen, *Nat. Phys.* (2019), 10.1038/s41567-019-0449-0.
- ⁴²J. Bardeen, L. N. Cooper, and J. R. Schrieffer, *Phys. Rev.* **108**, 1175 (1957).
- ⁴³R. Dynes, J. Garno, G. Hertel, and T. Orlando, *Phys. Rev. Lett.* **53**, 2437 (1984).
- ⁴⁴I. Giaever, *Phys. Rev. Lett.* **5**, 147 (1960).
- ⁴⁵J. P. Pekola, V. Maisi, S. Kafanov, N. Chekurov, A. Kemppinen, Y. A. Pashkin, O.-P. Saira, M. Möttönen, and J. Tsai, *Phys. Rev. Lett.* **105**, 026803 (2010).
- ⁴⁶N. W. Ashcroft and N. D. Mermin, *Solid state physics* (Saunders College, Philadelphia, 1976).
- ⁴⁷J. Goetz, F. Deppe, P. Eder, M. Fischer, M. Müting, J. Puertas Martínez, S. Pogorzalek, F. Wulschner, E. Xie, K. G. Fedorov, A. Marx, and R. Gross, *Quant. Sci. Tech.* **2**, 025002 (2017).
- ⁴⁸C. Gardiner and M. Collett, *Phys. Rev. A* **31**, 3761 (1985).
- ⁴⁹A. A. Clerk, M. H. Devoret, S. M. Girvin, F. Marquardt, and R. J. Schoelkopf, *Rev. Mod. Phys.* **82**, 1155 (2010).
- ⁵⁰S. Fan, W. Suh, and J. D. Joannopoulos, *J. Opt. Soc. Am. A* **20**, 569 (2003).
- ⁵¹M. Partanen, K. Y. Tan, S. Masuda, J. Govenius, R. E. Lake, M. Jenei, L. Grönberg, J. Hassel, S. Simbierowicz, V. Vesterinen, *et al.*, *Sci. Rep.* **8**, 6325 (2018).
- ⁵²M. Sandberg, C. Wilson, F. Persson, T. Bauch, G. Johansson, V. Shumeiko, T. Duty, and P. Delsing, *Appl. Phys. Lett.* **92**, 203501 (2008).
- ⁵³D. Schuster, A. Wallraff, A. Blais, L. Frunzio, R.-S. Huang, J. Majer, S. Girvin, and R. Schoelkopf, *Phys. Rev. Lett.* **94**, 123602 (2005).